

The SDSS DR6 Luminosity Functions of Galaxies

Antonio D. Montero-Dorta¹ & Francisco Prada¹

¹*Instituto de Astrofísica de Andalucía (CSIC), Granada, E-18008, Spain*

Accepted —. Received —; in original form —

ABSTRACT

We present number counts, luminosity functions (LFs) and luminosity densities of galaxies obtained using the Sloan Digital Sky Survey Sixth Data Release in all SDSS photometric bands. Thanks to the SDSS DR6, galaxy statistics have increased by a factor of ~ 9 in the u -band and by a factor of $\sim 4 - 5$ in the rest of the SDSS bands with respect to the previous work of Blanton et al. (2003b). In addition, we have achieved a high redshift completeness in our galaxy samples. Firstly, by making use of the survey masks, provided by the NYU-VAGC DR6, we have been able to define an area on the sky of high angular redshift completeness. Secondly, we guarantee that brightness-dependent redshift incompleteness is small within the magnitude ranges that define our galaxy samples. With these advances, we have estimated very accurate SDSS DR6 LFs in both the bright and the faint end. In the $^{0.1}r$ -band, our SDSS DR6 luminosity function is well fitted by a Schechter LF with parameters $\Phi_* = 0.90 \pm 0.07$, $M_* - 5 \log_{10} h = -20.73 \pm 0.04$ and $\alpha = -1.23 \pm 0.02$. As compared with previous results, we find some notable differences. In the bright end of the $^{0.1}u$ -band luminosity function we find a remarkable excess, of ~ 1.7 dex at $M_{^{0.1}u} \simeq -20.5$, with respect to the best-fit Schechter LF. This excess weakens in the $^{0.1}g$ -band, fading away towards the very red $^{0.1}z$ -band. A preliminary analysis on the nature of this bright-end bump reveals that it is mostly comprised of active galaxies and QSOs. It seems, therefore, that an important fraction of this exceeding luminosity may come from nuclear activity. In the faint end of the SDSS DR6 luminosity functions, where we can reach 1 – 1.5 magnitudes deeper than the previous SDSS LF estimation, we obtain a steeper slope, that increases from the $^{0.1}u$ -band, with $\alpha = -1.01 \pm 0.03$, to the very red $^{0.1}z$ -band, with $\alpha = -1.26 \pm 0.03$. These state-of-the-art results may be used to constrain a variety of aspects of star formation histories and/or feed-back processes in galaxy formation models.

Key words: catalogues - surveys - galaxies: luminosity function, mass function - large-scale structure of Universe.

1 INTRODUCTION

From the pioneering work of Humason (1956) and Sandage (1978), who measured redshifts of bright galaxies from the Shapley-Ames photometric catalog Shapley & Ames (1932), much effort has been invested in mapping the luminous and matter contents of the Universe. The Center for Astrophysics survey (CfA, Huchra et al. 1983) is considered as the first proper redshift survey, specifically designed for cosmology studies. More important, from the first slice of about 1,000 galaxies the CfA Redshift Survey provided the community with observational evidence of an old theoretical, and at times controversial idea: the existence of a large scale structure of galaxies in the Universe (Davis et al. 1985). This first vision of cosmic complexity encouraged the development of new imaging and spectrometric technology and, consequently, gave rise to a number of other red-

shift surveys that followed different approaches and strategies. To name but a few, the Southern Sky Redshift Survey (SSRS, da Costa et al. 1988); the Perseus-Pisces catalog (Giovannelli & Haynes 1991) or the catalogs based on data from the Infrared Astronomical Satellite (IRAS). In the last decade, the emergence of multi-fiber spectrographs set the scene for larger and deeper redshift surveys. Examples of these are the Las Campanas Redshift Survey (LCRS, Shectman et al. 1996), consisting of 26,418 galaxies with an average redshift of $z \sim 0.1$; or the 2 degree Field Redshift Survey (2dF RS, Colless et al. 2001), with about 222,000 galaxies and covering a sky area of 1500 deg^2 . Finally, the Sloan Digital Sky Survey (SDSS, York et al. 2000) is the largest photometric and spectroscopic survey ever compiled, and represents the most accurate map of the nearby universe at $z \lesssim 0.3$. The SDSS Sixth Data Release (Adelman-McCarthy et al. 2008), that we use in this paper,

contains spectroscopic information for more than 1,000,000 galaxies and quasars which spread over 7425 deg^2 on the sky. Only in recent years, with surveys like the DEEP2 Galaxy Redshift Survey (Davis et al. 2003) or the VIMOS-VLT Deep Survey (VVDS, Le Fevre et al. 2003), have we reached the stage where we can study the galaxy population in the distant ($z \sim 1$) Universe. Other high- z surveys are currently being completed.

The advances in the survey field also made it necessary to develop data reduction pipelines and analysis tools to process and understand increasingly larger data sets. These days, cosmologists use a number of statistics to characterize, for a particular survey, the distribution of galaxies in three-dimensional space. Number counts, selection functions, luminosity functions or correlation functions are just a few examples. In this work we focus on the number counts and the luminosity functions of galaxies, that we draw from the SDSS DR6. Number counts, which describe the distribution of fluxes of galaxies, have been calculated for a number of surveys. The general consensus is that, in the close-by universe, galaxy number counts look like what we expect from an euclidean, not-evolved Universe. Yasuda et al. (2001) obtained number counts for the SDSS Commissioning Data in all ugriz bands. Norberg et al. (2002) provided number counts for the 2dF survey in the b_j band. Feulner et al. (2007) not only estimated galaxy number counts for a set of catalogs based on the Munich Near-Infrared Cluster Survey (MUNICS, Drory et al. 2001) but also presented a complete revision of this subject in the literature (see their Figure 8). In contrast to galaxy number counts, the luminosity function (LF), which is the number density of galaxies per unit absolute magnitude, has been historically a rather controversial issue. For example, Marzke et al. (1994) - using the CfA RS -, Norberg et al. (2002) - 2dF RS - and Blanton et al. (2003b) - SDSS DR2-, all obtained very different results.

Both the luminosity function and the luminosity density of galaxies are observational signs of the process of galaxy formation and evolution. A precise determination of these statistics is needed to constrain current theories. Consequently, new discoveries in observational cosmology could make a strong impact in our understanding of the physical processes that drive the birth and life of galaxies in the Universe. Nowadays, state-of-the-art models of galaxy formation invoke a number of galactic "mechanisms", which are connected through the so-call feed-back processes. Disentangling these relations is an ambitious but crucial task in modern Cosmology. In this sense, the semi-analytic models of galaxy formation (SAMs, e.g. Croton et al. 2006), which are embedded in N-body simulations like the Millennium Run (see Springel et al. 2005), are a very useful tool for cosmologists. These SAMs are a good ground for testing new theoretical ideas and understanding their observational implications.

The main purpose of this work is to take advantage of the large increase in the galaxy statistics thanks to the SDSS DR6 to obtain the number counts, LFs and luminosity densities of galaxies in the nearby universe. We intend to shed light both in the faint end of the LF, where most discrepancies come from, and in the bright-end, where statistics have always been poor and errors, consequently large. In section 2 we briefly describe the SDSS DR6, discuss our sample selection and comment on redshift completeness. In

section 3 we present our results on the number counts, the LFs and the luminosity densities of galaxies in each one of the SDSS photometric bands. Finally, in Section 4 we discuss our results and in Section 5 we present a summary of our work. Throughout this paper, unless otherwise stated, we assume a standard Λ CDM concordance cosmology, with $\Omega_m = 0.3$, $\Omega_\Lambda = 0.7$, $w = -1$, and $h = 1$. In addition, we use AB magnitudes.

2 THE SLOAN DIGITAL SKY SURVEY DATA RELEASE 6. DATA SAMPLES SELECTION AND REDSHIFT COMPLETENESS

In this work, we use the SDSS Sixth Data Release (Adelman-McCarthy et al. 2008). This data set completes the North Galactic Cap, containing photometric information of ~ 290 million objects over 9583 deg^2 . Around 1.27 million objects were selected for spectroscopy, covering an area of 7425 deg^2 on the sky. Important for this work, spectroscopy is available for $\sim 1,000,000$ galaxies down to magnitude $r \sim 17.77$ (York et al. 2000; Stoughton et al. 2002). Detailed information about the SDSS DR6 can be found in Adelman-McCarthy et al. (2008).

The SDSS DR6 is the largest survey of the nearby universe publicly available. The SDSS collaboration have successively extended their catalogs since the times of the SDSS Early Data Release and, consequently, improved enormously our capability of mapping the universe up to redshift $z \sim 0.25$. A few years ago, Blanton et al. (2003b) used the SDSS DR2 to estimate the luminosity function of galaxies. In this work, thanks to the SDSS DR6, the size of our samples has risen by a factor ~ 9 in the very blue u-band and by a factor $\sim 4 - 5$ in the other bands (g, r, i and z). This huge enhancement in the statistics will be especially critical in the bright end of the LF, where statistics have always been poor in the past. In addition, we also expect to reach deeper magnitudes in the faint end with respect to previous works. Galaxy number counts can also be estimated with significantly more accuracy. It is therefore well justified to update the current knowledge on the number counts, luminosity functions and luminosity densities of galaxies in the close-by Universe.

2.1 Data samples selection

In this section, we describe the selection of our galaxy samples. We have drawn our samples from the NYU Value Added Galaxy Catalog DR6 Large Scale Structure sample (Blanton et al. 2005). The NYU-VAGC is a compilation of galaxy catalogs cross-matched to the SDSS that includes a number of useful quantities derived from the photometric and the spectroscopic catalogs (such as K-corrections or absolute magnitudes). It also incorporates a precise and user-friendly description of the geometry of the survey, which has never been used in previous SDSS LF works.

Before we proceed with the sample selection, we will describe how we built our Parent Sample from the NYU-VAGC LSS sample. The Parent Sample is the galaxy catalog from which we extract all samples that we use in this work. Firstly, we take all objects that satisfy the criteria of

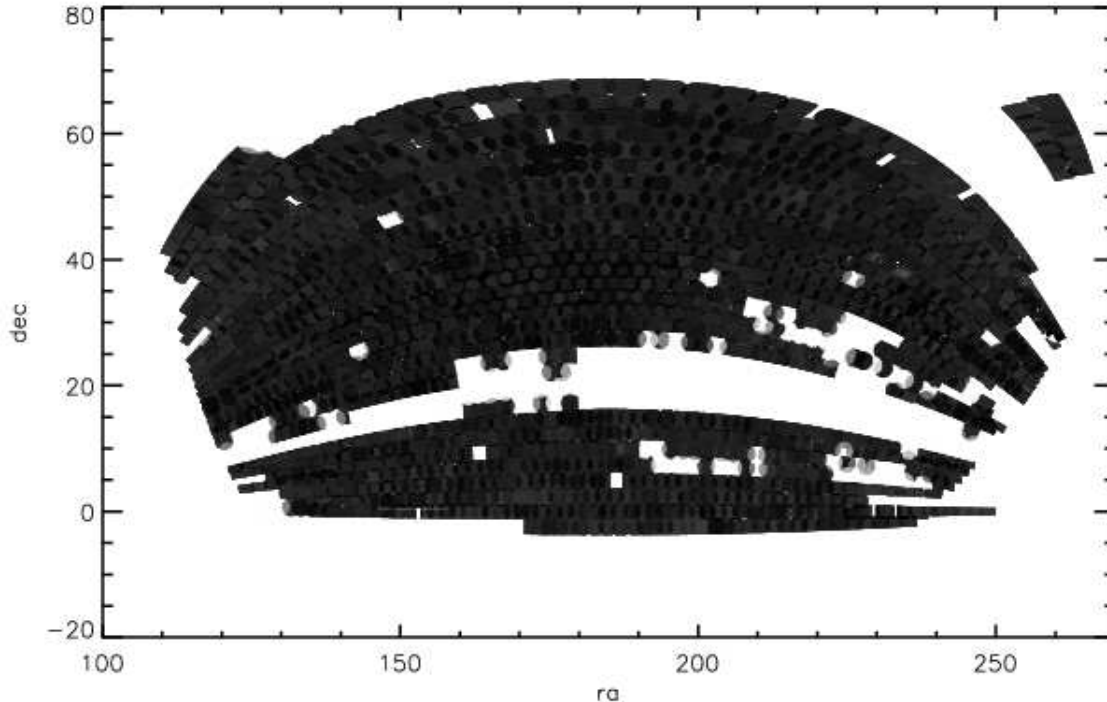


Figure 1. Angular redshift completeness of the SDSS DR6 spectroscopic catalog in the right ascension range $110^\circ < RA < 270^\circ$, that encompasses $\sim 99\%$ of the survey. Each polygon in the plot is an area of constant completeness. Polygons are also color-coded in white to black tones, meaning from 0% to 100% completeness.

the SDSS Main Galaxy Sample (Strauss et al. 2002). Secondly, we make use of the survey masks, provided by the NYU-VAGC, to define our *high-completeness survey window* (hereafter, HCSW). In this paper we deal with number counts and luminosity functions in the entire SDSS DR6 spectroscopic catalog. These tasks require knowing the effective area covered on the sky by the sample. In practice, redshift completeness, which is the fraction of galaxies with a successful redshift measurement, is far from being uniform across the sky. In Figure 1, we show the angular sky redshift completeness of the SDSS DR6 spectroscopic catalog for a major part of the survey ($\sim 99\%$), just excluding objects outside the range $110^\circ < RA < 270^\circ$, for the sake of clarity. The plot has been pixelized so that each pixel - or polygon - is an area of constant completeness. Polygons are also color-coded in white to black tones, the latter meaning 100% completeness. In order to avoid overestimating the area covered on the sky by our samples, the HCSW is defined so that redshift completeness is at least 80% in every polygon. Only galaxies lying in these polygons are included in our Parent Sample.

With these first restrictions our Parent Sample is comprised of 947,053 galaxies that spread over 6428.32 deg^2 on the sky. From this catalog, each sample is drawn by applying the following cuts to the redshift and apparent magnitude:

- $m_{min}(j) < m(j) < m_{max}(j)$
- $z_{min}(j) < z(j) < z_{max}(j)$

where $j = u, g, r, i, z$. In Table 1 we show lower and upper

| Band | Number | m_{min} | m_{max} | z_{min} | z_{max} |
|------|---------|-----------|-----------|-----------|-----------|
| u | 192,068 | 16.45 | 19.00 | 0.02 | 0.19 |
| g | 241,719 | 14.55 | 17.91 | 0.02 | 0.16 |
| r | 516,891 | 13.93 | 17.77 | 0.02 | 0.22 |
| i | 429,173 | 13.55 | 17.24 | 0.02 | 0.22 |
| z | 414,828 | 13.40 | 16.97 | 0.02 | 0.23 |

Table 1. Number of galaxies and limits in apparent magnitude and redshift of each SDSS photometric band sample. Motivation for each cut is discussed in section 2.1.

limits of these quantities along with the number of galaxies for each sample.

At this point, it is convenient to clarify the motivation for each cut. The apparent magnitude limits of Table 1 are set to ensure that the effect of redshift incompleteness is small in our SDSS galaxy samples. In the bright end, brightness-dependent redshift incompleteness starts to be important at $r \lesssim 15$. In the faint end, redshift incompleteness in all SDSS bands is dominated by the intrinsic faint limit of the Main Galaxy Sample (Strauss et al. 2002), i.e. $r = 17.77$. In order to choose these apparent magnitude limits, we have made use of the SDSS galaxy number counts, that will be properly discussed in Section 3.1. For each galaxy sample, we have taken the magnitude range where the number of galaxies rises at constant rate in each SDSS band, with a 0.1-dex deviation allowance (see Figure 4, where galaxy number counts have been scaled by an euclidean, not-evolved model). Within these limits, we have

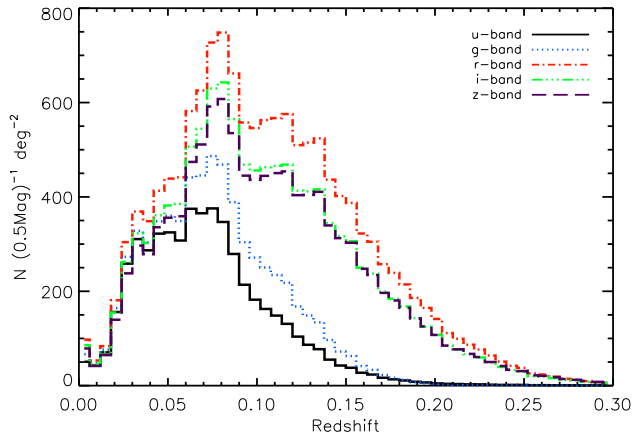


Figure 2. Redshift distributions in all SDSS photometric bands.

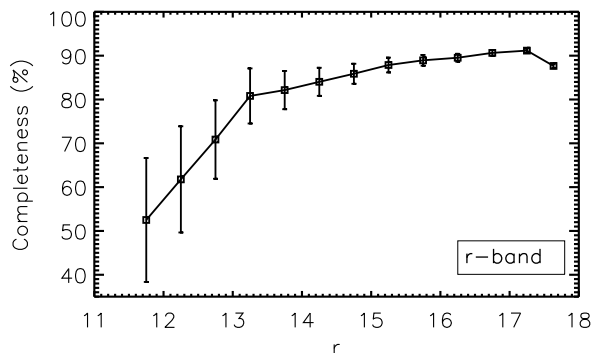


Figure 3. Redshift completeness vs. apparent magnitude in the r-band. At $r \lesssim 14$ completeness decreases sharply. Errors have been estimated by propagating the poissonian uncertainties to the redshift completeness.

estimated that redshift completeness is $\sim 85\%$ in all SDSS bands. In Section 2.2, we will discuss on redshift incompleteness issues in the SDSS in more detail.

In Figure 2, we show the redshift distribution for the Parent Sample in each SDSS photometric band. This figure illustrates the motivation for the redshift limits given in Table 1. The lower redshift limit is set to $z = 0.02$ to avoid the redshift incompleteness that affects the very bright and nearby galaxies. The upper redshift limit corresponds to the redshift at which 95% of objects are selected in each sample and is set for consistency.

2.2 Redshift Completeness

It is well known that the brightest galaxies in the SDSS catalogs are affected by a severe redshift incompleteness. This effect is especially important for nearby galaxies. Apparently large and complex objects represent a major task for the photometric SDSS pipelines (Strauss et al. 2002). In addition, and affecting the entire magnitude range, is the so-called *fiber collisions problem*. This source of incompleteness is due to the fact that fibers cannot be placed closer than $55''$. The consequence of this limitation in the SDSS

data is estimated in a 6% incompleteness by Strauss et al. (2002).

In Figure 3, we show how redshift completeness varies with apparent magnitude in the r-band. At $r \simeq 14$, redshift completeness falls from $\sim 85\%$ to $\sim 50\%$ at $r \simeq 12$. In the faint end, however, it reaches a plateau at 90% - down to $r \simeq 17.8$ -, which is in agreement with Strauss et al. (2002). In the rest of the SDSS bands, redshift completeness not only decreases in the bright end, but also in the faint end. This is due to the intrinsic r-band faint limit of the Main Galaxy Sample at $r = 17.77$. Interestingly, the apparent magnitude, $m_{min}(j)$, at which this decrease occurs varies between bands as a result of the dispersion in the colors of galaxies. We have checked that, by imposing $m_{max}(j) > m(j) > m_{min}(j)$, we ensure that each galaxy sample is approximately 85% complete in any magnitude bin.

Another aspect of redshift completeness that should be carefully taken into account is its angular variation. As we discussed above, a precise estimation of the area covered in the sky by our samples is needed in order to calculate number counts and luminosity functions of galaxies. We ensure here that we do not overestimate this area by defining a region, the HCSW, in which redshift completeness is at least 80%. The HCSW covers 6428.32 deg^2 , about 90% of the entire sky coverage of the SDSS DR6 spectroscopic catalog. As we can see in Figure 1, the SDSS DR6 sky coverage is patched with areas where no redshift was measured at all. These regions cover a total of 623.5 deg^2 on the sky.

Finally, we cannot discard the possibility that the SDSS spectroscopic catalog is incomplete for very low surface brightness objects, i.e. $\mu_{r,50} \gtrsim 24$. (see Strauss et al. 2002) The presence of this selection effect in the data could in principle affect our results. However, we have evidence that the surface brightness of most galaxies in the SDSS, and consequently in our galaxy samples, is far greater than $\mu_{r,50} \simeq 24$ (Blanton et al. 2003b).

3 RESULTS

3.1 Number counts

In Figure 4 we plot with different symbols the logarithm of the number of galaxies per unit area and apparent magnitude (actually, half magnitude), scaled by an euclidean model for all SDSS bands. We choose, arbitrarily, the following model for euclidean counts:

$$N_{euclidean} = 10^{0.6(x-18)} \quad (1)$$

where x is replaced by the apparent magnitude in each SDSS band.

In the r-band, galaxy number counts increase by a factor of about 10 from $r \sim 12$ to $r \sim 13.5$. This magnitude range is strongly affected by redshift incompleteness, as discussed above (see also Figure 3). From $r \sim 14$ to $r \sim 18$, counts rise at approximately the same rate as that of the model (Equation 1). At $r \sim 18$, where the SDSS spectroscopic faint-end limit is set ($r = 17.77$), galaxy number counts fall sharply.

In the rest of the bands, the behavior is very similar in the bright end and it is also due to redshift incompleteness. In the z-band, counts start to follow the euclidean model at $z \sim 13.5$. In the i-band, this happens at $i \sim 13.5$; in the

| Band | Apparent magnitude limits | Redshift limits | Slope |
|------|---------------------------|-------------------|-------|
| u | $16.45 < u < 19.00$ | $0.02 < z < 0.19$ | 0.627 |
| g | $14.55 < g < 17.91$ | $0.02 < z < 0.16$ | 0.608 |
| r | $13.93 < r < 17.77$ | $0.02 < z < 0.22$ | 0.610 |
| i | $13.55 < i < 17.24$ | $0.02 < z < 0.22$ | 0.611 |
| z | $13.40 < z < 16.97$ | $0.02 < z < 0.23$ | 0.626 |

Table 2. Slope in units of mag^{-1} of galaxy number counts within the apparent magnitude and redshift limits of each sample. Within these ranges, number counts are consistent with an Euclidean, not-evolved Universe.

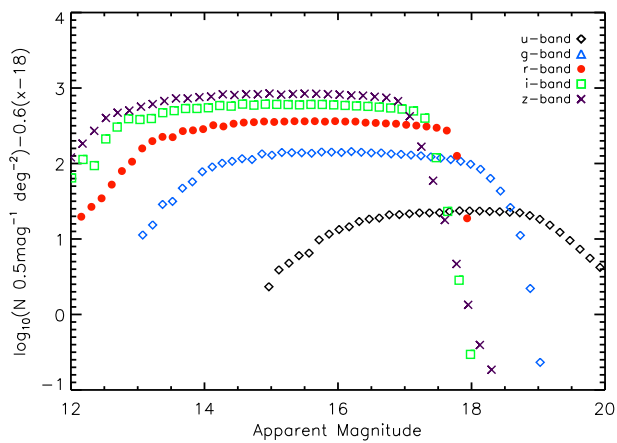


Figure 4. Galaxy number counts in all SDSS bands scaled by an euclidean model in bins of half a magnitude. Poissonian errors are of similar size as symbols, so they are not shown.

g-band, at $g \sim 14.5$ and, in the u-band, at $u \sim 16.5$. In the faint end, galaxy number counts fall at $u \sim 19$, $g \sim 18$, $i \sim 17$ and $z \sim 17$. This decrease is obviously less pronounced than in the r-band. This reflects the fact that the color-magnitude relation is not univoque. In addition, the dispersion in this relation is considerably larger for $u - r$ colors than it is for $r - z$ colors (Blanton et al. 2003a). As seen in Figure 4, the slope of the faint-end decrease in the galaxy number counts is considerably steeper in the u and g-bands than it is in the redder bands.

Number counts are consistent with an Euclidean, not-evolved Universe in all SDSS bands within the magnitude and redshift ranges given in Table 1. Within these ranges, the slopes in units of mag^{-1} of the SDSS DR6 galaxy number counts are listed in Table 2. Although discrepancies exist with respect to the euclidean model, these are probably smaller than the expected uncertainty in the determination of the apparent magnitude and redshift of each galaxy in the SDSS.

Our results for the nearby universe are in agreement with a number of previous works (see Feulner et al. 2007 for a review). However, only Yasuda et al. (2001) obtained galaxy number counts for SDSS data. The authors used imaging data taken only during the commissioning phase of the SDSS. They found an euclidean-like behavior up to magnitude $m_{\min} \sim 12$ - except for the u-band, where $m_{\min} \sim 14$ - (see their Figure 8). The lack of galaxies in the very bright

end of Figure 4 with respect to photometric number counts from Yasuda et al. (2001) is partially due to the strong redshift incompleteness that affects the SDSS spectroscopic catalog in these magnitude ranges (see Section 2.2). However, our results and those from Yasuda et al. (2001) are not directly comparable. Firstly, they used a very limited sample, in terms of sky coverage ($\sim 230 \text{ deg}^2$). Secondly, comparing spectroscopic and photometric results is always tricky.

3.2 Luminosity Functions

In order to estimate the luminosity function of galaxies in each SDSS photometric band, we take absolute magnitudes and K-corrections from the NYU VAGC DR6 LSS catalog. Following Blanton et al. (2003b), absolute magnitudes are calculated with the SDSS photometric bands shifted to $z = 0.1$. With this convention, the absolute magnitude of a galaxy in a given band shifted to $z = 0.1$, $M_{0.1j}$, would be constructed from its apparent magnitude at $z = 0$, m_j , and its redshift z as follows:

$$M_{0.1j} = m_j - 5\log_{10}h - DM(z) - K_{0.1j}(z) \quad (2)$$

where $DM(z)$ is the distance modulus (which depends also on the cosmological parameters) and $K_{0.1j}(z)$, the K-correction for the galaxy in the shifted band $^{0.1}j$. Blanton et al. (2003b) included another correction in Expression 2 to account for the evolution of the luminosity of a galaxy from redshift z to $z = 0$, the so-called evolution correction. However, we expect this correction to be very small within the redshift ranges that we have considered here (see also Section 4). In Figure 5, we show the distribution of K-corrected absolute magnitudes in each galaxy sample. The shape of the absolute magnitude distribution is very similar in all SDSS bands: a gaussian-like distribution slightly skewed to fainter magnitudes. However, mean values move towards bright-end bins from $^{0.1}u$ -band - $M_{0.1u} \sim -18$ - to $^{0.1}z$ -band - $M_{0.1z} \sim -21.5$, which is consistent with the fact that red objects are, on average, brighter than blue objects. In Figure 6, we also show the bimodal $^{0.1}u - ^{0.1}r$ color distribution of galaxies in our $^{0.1}r$ -band sample. With a dashed line we represent the demarcation commonly used to separate red and blue objects (see Strateva et al. 2001).

We use the Stepwise Maximum Likelihood Method (SWML; Efstathiou et al. 1988) to estimate the LF of galaxies, that is commonly expressed as $\Phi(L)$. This technique does not rely on any assumption about the shape of $\Phi(L)$ and is considered as the most reliable estimator of the LF. For more details about this method see Efstathiou et al. (1988) and Norberg et al. (2002). The SWML requires an independent estimation of the number density of galaxies, i.e. the normalization constant, n . We use the following prescription proposed by Davis & Huchra (1982) based on the selection function of each galaxy, $\phi(z_i)$, and the maximum volume encompassed by the sample, V_{\max} :

$$n = \frac{1}{V_{\max}} \sum_i \frac{1}{\phi(z_i)} \quad (3)$$

In Figure 7 we show the SWML estimate of the SDSS DR6 LF in the $^{0.1}r$ -band. In addition, we over-plot with a dashed line the best-fit Schechter function (Schechter 1976), which has the following shape:

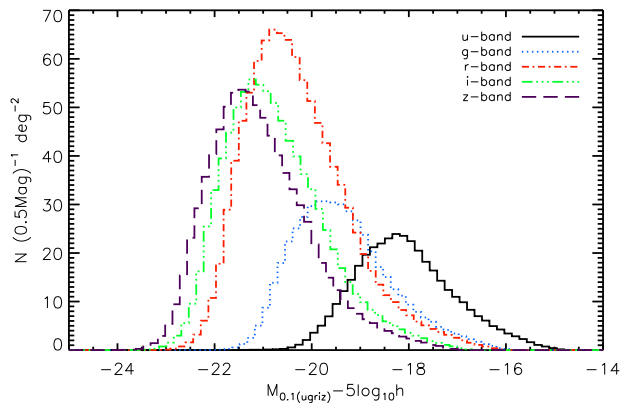


Figure 5. Absolute magnitude distribution in each sample. Although the shape of the distributions is very similar, mean values move towards bright-end magnitude bins from $^{0.1}u$ -band to $^{0.1}z$ -band, as red objects are, on average, brighter than blue objects.

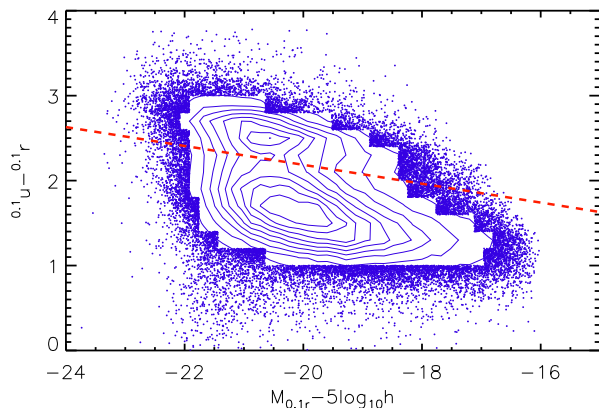


Figure 6. The $(^{0.1}u - ^{0.1}r)$ color-magnitude diagram in the $^{0.1}r$ -band. The dashed line represents the demarcation commonly used to separate red and blue galaxies.

$$\Phi(M) = 0.4 \log(10) \Phi_* 10^{-0.4(M-M_*)(\alpha+1)} \exp \left[-10^{-0.4(M-M_*)} \right] \quad (4)$$

where α , M_* and Φ_* are the three parameters to fit. Values of these parameters for the best-fit Schechter function are given in Table 3. For comparison, we also show in Figure 7 the LF of Blanton et al. (2003b) with a solid line. This comparison will be addressed in the Discussion section. To calculate errors in the SWML estimates of the LF we perform a bootstrapping analysis using 1,000 random sub-samples of 1/3 of the number of objects in each sample. In Figure 7, shaded regions represent the 1σ uncertainty obtained from this method.

Due to the big number statistics that we have, with about 500,000 galaxies in the $^{0.1}r$ -band, errors are only significant in the very bright end of the LF. In the faint end, we can go down to $M_{0.1r} \sim -16$, which means that we can build the LF with unprecedented precision within a very

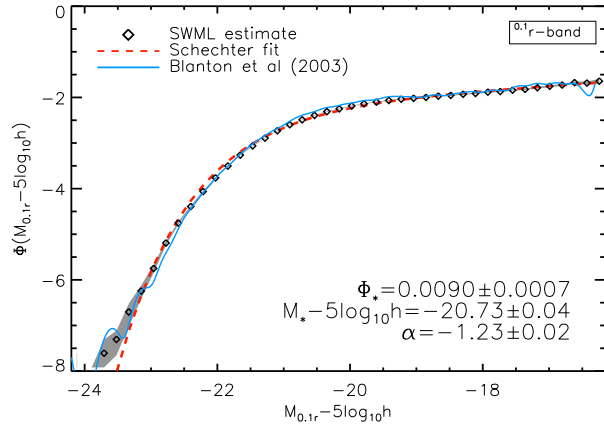


Figure 7. The $^{0.1}r$ -band SDSS DR6 Luminosity Function. The SWML LF estimate is shown in diamonds. The dashed line represents the best-fit Schechter function and the solid line, the $^{0.1}r$ -band LF from Blanton et al. (2003b). Best-fit values of Schechter parameters α , M_* and Φ_* are also shown in the figure. Shaded regions represent the 1σ uncertainty calculated using a bootstrapping technique.

large range of magnitudes. As we will see below, the above statements hold for all SDSS bands. Our $^{0.1}r$ -band LF is reasonably well fitted by a Schechter LF with a faint-end slope $\alpha = -1.23$. It is only in the very bright end where this best-fit Schechter LF starts to underestimate our LF. At $M_{0.1r} \lesssim -23.5$, statistics are poor and errors become increasingly large.

In Figure 8 we present, in the same way as in Figure 7, SWML estimates of the LF in bands $^{0.1}u$, $^{0.1}g$, $^{0.1}i$ and $^{0.1}z$, as well as their corresponding best-fit Schechter LF. Values of best-fit Schechter parameters are also given in Table 3. As in the $^{0.1}r$ -band, errors are only significant in the very bright end of $^{0.1}u$, $^{0.1}g$, $^{0.1}i$ and $^{0.1}z$ -band luminosity functions. In addition, we can go down to very faint magnitudes without losing precision.

In the very blue $^{0.1}u$ -band, the shape of our SDSS DR6 LF is consistent with a Schechter LF with an almost flat faint-end slope (corresponding to $\alpha = -1.01$). However, in the bright end, we find a remarkable excess with respect to the best-fit Schechter LF. This excess, of ~ 1.7 dex at $M_{0.1u} \approx -20.5$, is very significant within the magnitude range $-20.5 < M_{0.1u} \lesssim -22$. In the $^{0.1}g$ -band, the bright-end bump weakens considerably, but it is probably still significant, even though errors are large according to our bootstrapping analysis. In this band, our SDSS LF is very well fitted by a Schechter LF with a positive faint-end slope, corresponding to $\alpha = -1.10$. Only in the very bright-end, where the excess is still noticeable, do we find some discrepancy. Below, we provide a preliminary analysis and discussion on the nature of the $^{0.1}u$ -band LF bright-end bump, that may have important implications in terms of galaxy formation and evolution.

In the redder bands we find a positive faint-end slope, corresponding to $\alpha = -1.16$ in the $^{0.1}i$ -band and $\alpha = -1.26$ in the $^{0.1}z$ -band. The bright-end bump has diminished substantially in the $^{0.1}i$ -band and has disappeared in the very red $^{0.1}z$ -band. It is interesting to note that, from the $^{0.1}u$ -band to the $^{0.1}z$ -band, the shape of the SWML estimate of

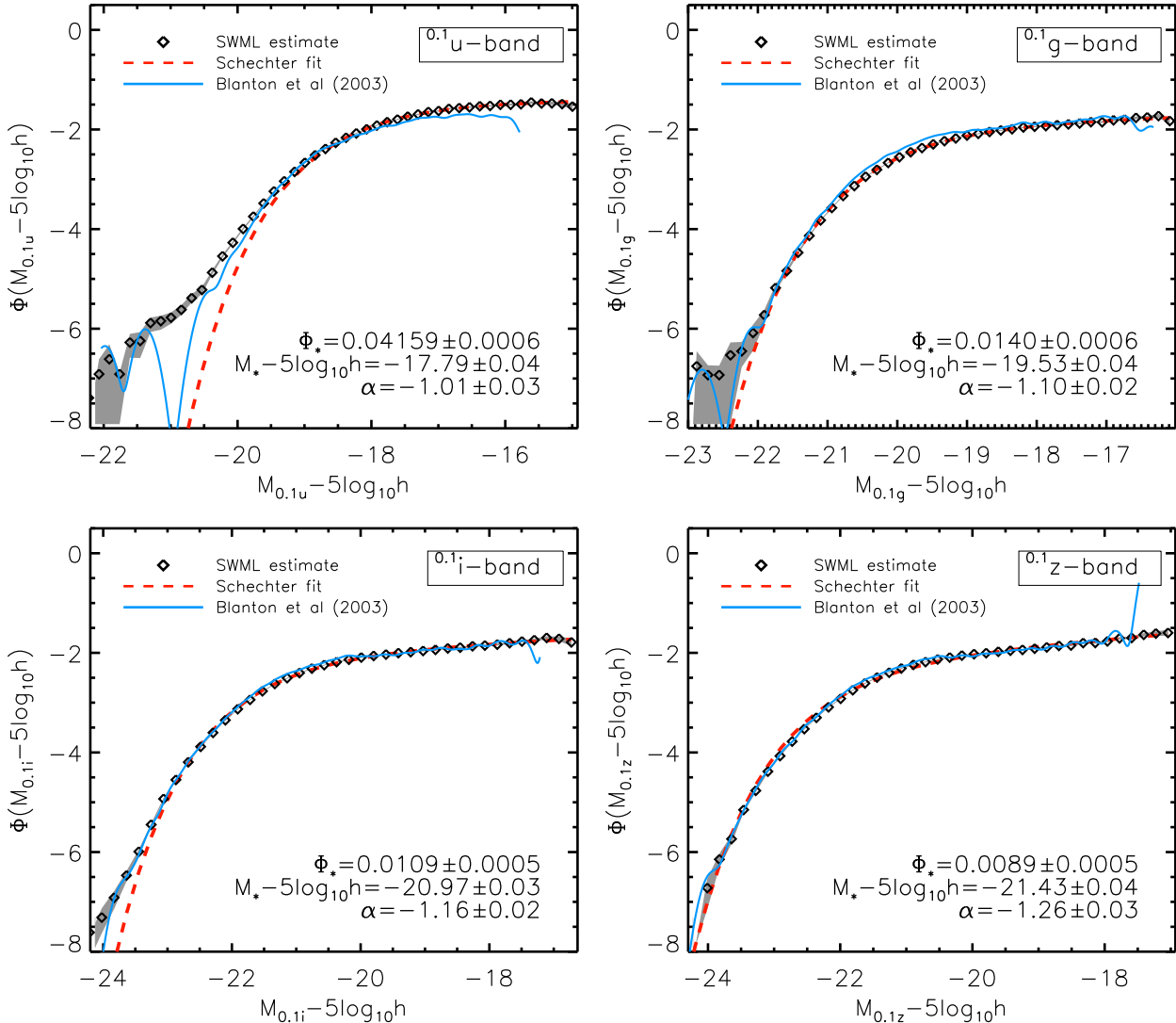


Figure 8. The SDSS DR6 Luminosity Functions in bands $^{0.1}u$, $^{0.1}g$, $^{0.1}i$ and $^{0.1}z$. SWML LF estimates are shown in diamonds and best-fit Schechter functions are represented by dashed lines. In addition, we over-plot in each panel the LF from Blanton et al. (2003b). Best-fit values of Schechter parameters α , M_* and Φ_* are also shown. Shaded regions represent the 1σ uncertainty calculated using a bootstrapping technique.

the SDSS LF changes following a clear pattern. The faint-end slope increases towards the redder bands (see Table 3), being almost flat in the $^{0.1}u$ -band and remarkably steep in the $^{0.1}z$ -band. Conversely, the excess of bright galaxies with respect to the best-fit Schechter function diminishes towards redder bands. In principle, one might think that the strong bright-end excess in the $^{0.1}u$ -band fades progressively towards redder bands and only disappear completely in the $^{0.1}z$ -band. In this sense, the $^{0.1}r$ -band SDSS LF seems to slightly deviate from this trend. In the faint-end, we find a slope that is a bit larger than we could expect ($\alpha = -1.23$), but this could be just a consequence of the fact that the entire SDSS spectroscopic sample was selected in this band.

The bright-end bump that shows up clearly in the $^{0.1}u$ -band LF (and partially in the $^{0.1}g$ -band LF) is an interesting discovery that may have implications for our understanding of galaxy formation and evolution. In order to investigate

the nature of the objects that populate it, we have selected all galaxies brighter than -20.5 in the $^{0.1}u$ -band sample. We will hereafter refer to this sample, which is comprised of 422 objects, as the bright-end bump sample (BEBS).

We have visually inspected the spectra of all galaxies in the BEBS and classified them into three types. About 60% of objects have a typical QSO or Seyfert I spectrum, 27% of sources are classified as LINERs or Starburst (SB) and only $\sim 13\%$ of objects are galaxies with a bulge-like spectrum, and showing little or no signs of star formation. In Figure 9 we plot in the $(^{0.1}u - ^{0.1}r)$ vs. $M_{0,^{0.1}u}$ colour-magnitude diagram (CMD) of the $^{0.1}u$ -band sample the three types of BEBS galaxies discussed above. In general, these galaxies form a relatively tight sequence in the bright-end of the CMD, showing a considerable color dispersion. Note that, in contrast to Figure 6, density contours are now log-spaced and hence, these ob-

| This work | | | | Blanton et al. (2003) | | | |
|-----------|------------------------------|--------------------|------------------|-----------------------|------------------------------|--------------------|------------------|
| Band | $\Phi_*(10^{-2}h^3Mpc^{-3})$ | $M_* - 5log_{10}h$ | α | Band | $\Phi_*(10^{-2}h^3Mpc^{-3})$ | $M_* - 5log_{10}h$ | α |
| $^{0.1}u$ | 4.16 ± 0.06 | -17.79 ± 0.04 | -1.01 ± 0.03 | $^{0.1}u$ | 3.05 ± 0.33 | -17.93 ± 0.03 | -0.92 ± 0.07 |
| $^{0.1}g$ | 1.40 ± 0.06 | -19.53 ± 0.04 | -1.10 ± 0.02 | $^{0.1}g$ | 2.18 ± 0.08 | -19.39 ± 0.02 | -0.89 ± 0.03 |
| $^{0.1}r$ | 0.90 ± 0.07 | -20.73 ± 0.04 | -1.23 ± 0.02 | $^{0.1}r$ | 1.49 ± 0.04 | -20.44 ± 0.01 | -1.05 ± 0.01 |
| $^{0.1}i$ | 1.09 ± 0.05 | -20.97 ± 0.03 | -1.16 ± 0.02 | $^{0.1}i$ | 1.47 ± 0.04 | -20.82 ± 0.02 | -1.00 ± 0.02 |
| $^{0.1}z$ | 0.89 ± 0.05 | -21.43 ± 0.04 | -1.26 ± 0.03 | $^{0.1}z$ | 1.35 ± 0.04 | -21.18 ± 0.02 | -1.08 ± 0.02 |

Table 3. Values of Schechter parameters α , M_* and Φ_* of the best-fit Schechter function in all SDSS bands for this work and for Blanton et al. (2003b).

jects occupy an extremely underpopulated region in the CMD. In the left-hand plot, QSOs/Seyferts I show the smallest color dispersion and are, on average, the bluest: $\langle (^{0.1}u - ^{0.1}r) \rangle = 0.68$. Both LINERs/SBs (middle plot) and bulge-like galaxies (right-hand plot) show much larger color dispersion and are, on average, considerably redder, with $\langle (^{0.1}u - ^{0.1}r) \rangle = 1.07$ and $\langle (^{0.1}u - ^{0.1}r) \rangle = 0.91$, respectively. In the $^{0.1}u$ -band, bulge-like galaxies are, on average, the brightest among the BEBS galaxies: $\langle M_{0.1u} \rangle = (-20.97^{QSO/SI}, -20.77^{LIN/SB}, -21.03^{bulge})$.

We have checked that BEBS galaxies are typically at high redshift relative to the average redshift of the $^{0.1}u$ -band sample from which they are drawn. The mean redshift in the BEBS is $\langle z \rangle \sim 0.155$ while in the entire $^{0.1}u$ -band sample is $\langle z \rangle \sim 0.080$.

At this point, it is necessary to remark that this is a preliminary analysis. We have performed a rough classification of the BEBS galaxies, and this is still subject to some uncertainty. However, our aim is to provide a first approach to the nature of this population of objects. In Section 4 we speculate on possible implications of these results.

Finally, in Figure 10, we present, in the same way as in Figure 7 and Figure 8, SWML estimates of the SDSS $^{0.1}r$ -band LF for blue and red galaxies separately, as well as their corresponding best-fit Schechter LF. Values of best-fit Schechter parameters are also shown in the figure. The demarcation that we use to separate blue and red objects is represented by a dashed line in Figure 6. The SDSS $^{0.1}r$ -band LF of blue galaxies is well fitted by a Schechter LF with $\alpha = -1.36$. In contrast, the SDSS $^{0.1}r$ -band LF of red galaxies has a negative faint-end slope, corresponding with $\alpha = -0.81$. These results are consistent with a number of previous works. In the bright end, at $M_{0.1r} \lesssim -21.5$, the blue LF falls remarkably below the red LF.

3.3 Luminosity Densities

To estimate the luminosity density, ρ , in all SDSS bands, we integrate throughout the entire absolute magnitude ranges defined by the limits shown in Table 4. In this table we list ρ in all bands obtained using the SWML estimate of the luminosity functions shown in Figure 7 and Figure 8. Luminosity densities are expressed in $AB\ mags\ (Mpc^3h^{-1})^{-1}$. We also give in Table 4 the effective wavelength corresponding to each SDSS photometric band, λ_{eff} . Errors shown in this table have been calculated using a similar bootstrapping technique as that discussed in Section 3.2. We have

used 1000 random sub-samples of 1/3 the number of objects in each sample.

As expected, the luminosity density in the nearby universe increases with λ_{eff} , in absolute values. This means that the Universe, up to $z \sim 0.2$, is considerably more luminous in the red side of the spectrum than it is in the blue side. Our luminosity densities obtained using the SWML LF estimate are in good agreement with Blanton et al. (2003b) (see Table 4). Both estimates differ in less than 2% in any band.

However, it is necessary to note that the value of ρ is not too sensitive to small variations in the shape of the luminosity function. In Table 4, we also provide luminosity densities in each band obtained using the Schechter fits to the SWML LF estimates of the luminosity functions discussed in Section 3.2. The values of ρ obtained using the SWML estimates and those obtained from the Schechter fit differ in less than 1% in each band.

4 DISCUSSION

The main results presented in this work are the SDSS DR6 Luminosity Functions of galaxies in the nearby universe. A few years ago, Blanton et al. (2003b) used an early version of the SDSS (DR2) to calculate the SDSS galaxy LFs. Now, with the SDSS DR6 available, galaxy statistics have improved by a huge factor of ~ 9 in the very blue $^{0.1}u$ -band and by a factor of $\sim 4 - 5$ in the rest of the SDSS photometric bands. Moreover, we have ensured a high redshift completeness in our galaxy samples. Firstly, we have defined an area on the sky of high angular redshift completeness by making use of the survey masks, provided by the NYU-VAGC. Secondly, we guarantee that the effect of brightness-dependent redshift incompleteness is negligible within the magnitude ranges that define our galaxy samples. These advances make our SDSS DR6 LFs substantially more precise than those from Blanton et al. (2003b) at both the bright and the faint end. This said, the LFs of Blanton et al. (2003b) are compatible with our results. However, notable differences, which are surely physically significant, exist. In the bright end of the blue bands LFs (especially in the $^{0.1}u$ -band) we find a remarkable excess, which was very noisy in Blanton et al. (2003b) due to their lack of statistics. In the faint end, we obtain steeper slopes in all SDSS bands, especially in the $^{0.1}u$ -band, where the DR6 statistics allow us to go about 1 - 1.5 magnitudes deeper as compared to Blanton et al. (2003b). If the huge improvement in the statistics and/or

| Band | $\lambda_{eff}(\text{\AA})$ | Absolute Magnitude Range | $\rho_{SWML} + 2.5\log_{10}h$ | $\rho_{Schechter} + 2.5\log_{10}h$ | $\rho_{Blanton2003} + 2.5\log_{10}h$ |
|---------|-----------------------------|-------------------------------|-------------------------------|------------------------------------|--------------------------------------|
| 0.1_u | 3216 | $-23.06 < M_{0.1_u} < -14.63$ | -14.288 ± 0.013 | -14.264 | -14.10 ± 0.15 |
| 0.1_g | 4240 | $-24.93 < M_{0.1_g} < -15.63$ | -14.910 ± 0.012 | -14.906 | -15.18 ± 0.03 |
| 0.1_r | 5595 | $-26.03 < M_{0.1_r} < -16.16$ | -15.769 ± 0.012 | -15.767 | -15.90 ± 0.03 |
| 0.1_i | 6792 | $-26.23 < M_{0.1_i} < -16.63$ | -16.113 ± 0.017 | -16.147 | -16.24 ± 0.03 |
| 0.1_z | 8111 | $-26.53 < M_{0.1_z} < -16.93$ | -16.500 ± 0.017 | -16.479 | -16.56 ± 0.02 |

Table 4. Luminosity densities in AB mags (Mpc^3h^{-1}) $^{-1}$ for all SDSS photometric bands calculated using the SWML estimate of the luminosity functions of Figure 7 and Figure 8 (ρ_{SWML}) and the Schechter LF best fits of Table 3 ($\rho_{Schechter}$). Absolute magnitude ranges of the integration and the effective wavelength corresponding to each band, λ_{eff} , are also provided. Errors in ρ_{SWML} have been calculated using a bootstrapping technique. In addition, we give for comparison the luminosity densities from Blanton et al. (2003b).

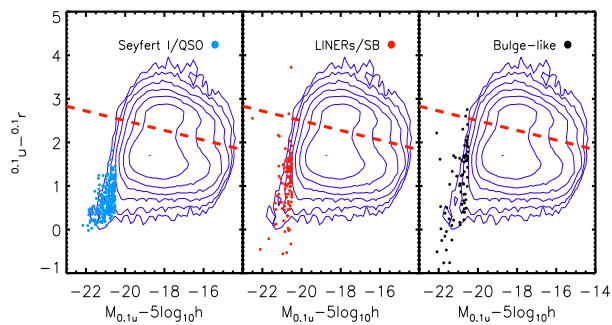


Figure 9. The $(0.1_u - 0.1_r)$ vs. $M_{0.1_u}$ color-magnitude diagram for the three types of bright-end bump galaxies considered: Seyferts I/QSO's (left-hand plot), LINER's/SB's (middle plot) and Bulge-like galaxies (right-hand plot). The underlying CMD of the entire 0.1_u -band sample from which BEBS galaxies are selected is shown with log-spaced contours.

the more accurate determination of the sample completeness were not behind this discrepancies, one possible explanation could come from the so-called evolution correction (Blanton et al. 2003b), which we have not taken into account in the determination of our absolute magnitudes. Because we are dealing with relatively nearby objects, it seems unlikely that this correction could modify our results significantly. It is worth mentioning at this point that relatively small variations in the shape of the LF, which are probably not physically significant - given the uncertainties we are dealing with -, may translate into considerable changes in the values of the best-fit Schechter parameters. It is not convenient, therefore, to make comparisons between different LFs by just looking at these best-fit Schechter parameters.

We have seen that the bright-end bump that we see in the blue bands (and marginally in the rest of the bands) is statistically very significant, according to our standard bootstrapping error analysis. Moreover, as we mentioned above, we also find clear - but noisy - evidence of its existence in Blanton et al. (2003b). We have also checked that this excess is not a consequence of any of the limits that we have imposed to define our samples. This is, therefore, a remarkable result that may have strong implications for galaxy evolution.

From a preliminary analysis on the nature of this bright-end bump in the 0.1_u -band LF, we have seen that it is mostly populated by star-forming and active galaxies ($\sim 85\%$). The

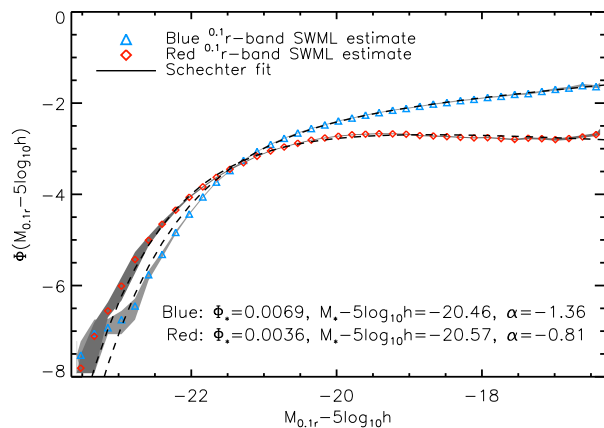


Figure 10. The 0.1_r -band SDSS DR6 Luminosity Function for blue and red galaxies separately. The SWML LF estimates are shown in diamonds. The dashed lines represents the best-fit Schechter function. Best-fit values of Schechter parameters α , M_* and Φ_* for both blue and red galaxies are also shown in the figure. Shaded regions represent the 1σ uncertainty calculated using a bootstrapping technique.

spectra of these galaxies seem consistent with what we expect from QSOs/Seyferts I ($\sim 60\%$) and LINERs/Starbursts ($\sim 25\%$). It seems, therefore, that an important fraction of the light that we receive from the brightest galaxies in the 0.1_u -band would come from nuclear activity. Only about 15% of galaxies in bright-end bump seem to be bulge-like galaxies. A more detailed study is needed, however, to fully understand the nature of this bright-end bump.

The implications of this new results could be investigated using semi-analytic models of galaxy formation and evolution (SAMs). With these models, we can, in principle, evaluate different processes and feed-back relations that could reproduce our results.

5 SUMMARY

In this work we make use of the SDSS Sixth Data Release to estimate the number counts, luminosity functions and luminosity densities of galaxies in all SDSS photometric bands. The SDSS DR6 is, by far, the most complete survey of the nearby universe, containing redshifts for $\sim 1,000,000$ galaxies down to magnitude $r \sim 17.77$ and covering ~ 7400 deg^2 on the sky. The huge increase in the galaxy statistics with

respect to the previous work of Blanton et al. (2003b) and the adequate treatment of both angular and brightness-dependent redshift completeness in our samples have allowed us to estimate the galaxy LFs of the nearby universe with unprecedented accuracy. In addition, we have calculated, for the first time, the SDSS galaxy number counts in all photometric bands using spectroscopic data. Luminosity densities in all SDSS bands have also been computed.

The main results of this work can be summarized as follows:

- The SDSS DR6 galaxy number counts in all SDSS photometric bands are consistent with an Euclidean, not-evolved Universe within a magnitude range that is limited by redshift incompleteness in the bright end and by the intrinsic apparent magnitude r-band limit of the survey, $r = 17.77$, in the faint end.

- The SDSS DR6 LF of galaxies in the very blue $^{0.1}u$ -band deviates considerably from that of Blanton et al. (2003b). This discrepancy can be explained by their lack of statistics, which has increased by a factor of ~ 9 thanks to the SDSS DR6. In the faint end, where we can reach about 1 to 1.5 magnitudes deeper without losing accuracy, our SDSS DR6 LF is considerably steeper than that of Blanton et al. (2003b). More interesting, in the bright end we find a remarkable excess, of ~ 1.7 dex at $M_{0.1u} \simeq -20.5$ with respect to the best-fit Schechter LF. This bright-end bump is very strong in the $^{0.1}u$ -band and weakens in the $^{0.1}g$ -band, fading away towards the very red $^{0.1}z$ -band.

- We conclude that the SDSS DR6 LFs of galaxies in the $^{0.1}g$, $^{0.1}r$, $^{0.1}i$ and $^{0.1}z$ bands are also compatible with Blanton et al. (2003b), considering the large increase in the statistics thanks to the SDSS DR6, of a factor $\sim 4 - 5$ in these bands. Some significant differences exist, however, especially in the faint end, where we find a slightly steeper slope and we can reach about 1 magnitude deeper without losing precision.

- A preliminary analysis of the origin of the bright-end bump seen in the $^{0.1}u$ -band SDSS DR6 LF reveals that it is comprised of QSO and Seyferts I galaxies ($\sim 60\%$), Starburst and LINERs ($\sim 25\%$) and bulge-like galaxies ($\sim 15\%$). It seems, therefore, that a big fraction of this exceeding luminosity might come from nuclear activity.

- The $^{0.1}r$ -band SDSS DR6 LF of blue galaxies is consistent with a Schechter LF with a remarkably steep faint-end slope, corresponding to $\alpha = -1.36$. The $^{0.1}r$ -band SDSS DR6 LF of red galaxies has, however, a slightly decreasing faint-end slope, corresponding to $\alpha = -0.81$.

- The SDSS DR6 luminosity densities of galaxies are in very good agreement with Blanton et al. (2003b) in all photometric bands, since they are integrated quantities.

The state-of-the-art results presented in this paper may be used to constrain a variety of aspects of star formation histories or feed-back processes in galaxy formation models. However, much effort is still needed in the survey field to fully understand the mechanisms that drive the evolution of galaxies in the Universe. This is especially necessary at high- z , where statistics are still very poor.

ACKNOWLEDGEMENTS

ADMD is supported by the Ministerio de Educación y Ciencia of the Spanish Government (MEC) through FPI grant AYA2005-07789. ADMD and FP acknowledge the MEC for their financial support through PNAYA2005-07789.

We would like to especially thank Michael Blanton for providing help on the calculation of the luminosity function and giving comments on the manuscript. We acknowledge Michael Blanton and David Hogg as the corresponding authors of the NYU-VAGC DR6.

We also want to thank Jonatan Hernández-Fernández, Víctor M. Muñoz Marín, Anatoly Klypin and Hans-Walter Rix for stimulating scientific discussions. Finally, we thank Antonio J. Cuesta for providing technical help throughout the process of making this work.

Funding for the SDSS has been provided by the Alfred P. Sloan Foundation, the Participating Institutions, NASA, the NSF, the U.S. Department of Energy, the Japanese Monbukagakusho, and the Max Planck Society. The SDSS website is <http://www.sdss.org/>.

REFERENCES

- Adelman-McCarthy J. K., Agüeros M. A., Allam S. S., et al., 2008, *ApJS*, 175, 297
- Blanton M. R., Hogg D. W., Bahcall N. A., et al., 2003a, *ApJ*, 594, 186
- Blanton M. R., Hogg D. W., Bahcall N. A., et al., 2003b, *ApJ*, 592, 819
- Blanton M. R., Schlegel D. J., Strauss M. A., et al., 2005, *AJ*, 129, 2562
- Colless M., Dalton G., Maddox S., et al., 2001, *MNRAS*, 328, 1039
- Croton D. J., Springel V., White S. D. M., et al., 2006, *MNRAS*, 365, 11
- da Costa L. N., Pellegrini P. S., Sargent W. L. W., et al., 1988, *ApJ*, 327, 544
- Davis M., Efstathiou G., Frenk C. S., White S. D. M., 1985, *ApJ*, 292, 371
- Davis M., Faber S. M., Newman J., et al., 2003, in *Discoveries and Research Prospects from 6- to 10-Meter-Class Telescopes II*. Edited by Guhathakurta, Puragra. Proceedings of the SPIE, Volume 4834, pp. 161-172 (2003).. edited by P. Guhathakurta, vol. 4834 of Presented at the Society of Photo-Optical Instrumentation Engineers (SPIE) Conference, 161-172
- Davis M., Huchra J., 1982, *ApJ*, 254, 437
- Drory N., Feulner G., Bender R., et al., 2001, *MNRAS*, 325, 550
- Efstathiou G., Ellis R. S., Peterson B. A., 1988, *MNRAS*, 232, 431
- Feulner G., Goranova Y., Hopp U., et al., 2007, *MNRAS*, 378, 429
- Giovanelli R., Haynes M. P., 1991, *ARA&A*, 29, 499
- Huchra J., Davis M., Latham D., Tonry J., 1983, *ApJS*, 52, 89
- Humason M. L., 1956, *Vistas in Astronomy*, 2, 1620
- Le Fevre O., Vettolani G., Maccagni D., et al., 2003, in *Discoveries and Research Prospects from 6- to 10-Meter-Class Telescopes II*. Edited by Guhathakurta, Puragra. Proceedings of the SPIE, Volume 4834, pp. 173-182 (2003)..

- edited by P. Guhathakurta, vol. 4834 of Presented at the Society of Photo-Optical Instrumentation Engineers (SPIE) Conference, 173–182
- Marzke R. O., Huchra J. P., Geller M. J., 1994, *ApJ*, 428, 43
- Norberg P., Cole S., Baugh C. M., et al., 2002, *MNRAS*, 336, 907
- Sandage A., 1978, *AJ*, 83, 904
- Schechter P., 1976, *ApJ*, 203, 297
- Shapley H., Ames A., 1932, *Annals of Harvard College Observatory*, 88, 41
- Shectman S. A., Landy S. D., Oemler A., et al., 1996, *ApJ*, 470, 172
- Springel V., White S. D. M., Jenkins A., et al., 2005, *Nature*, 435, 629
- Stoughton C., Lupton R. H., Bernardi M., et al., 2002, *AJ*, 123, 485
- Strateva I., Ivezić Ž., Knapp G. R., et al., 2001, *AJ*, 122, 1861
- Strauss M. A., Weinberg D. H., Lupton R. H., et al., 2002, *AJ*, 124, 1810
- Yasuda N., Fukugita M., Narayanan V. K., et al., 2001, *AJ*, 122, 1104
- York D. G., Adelman J., Anderson Jr. J. E., et al., 2000, *AJ*, 120, 1579